ACI STRUCTURAL JOURNAL TECHNICAL PAPER

Title no. 106-S83

Size-Scale Effects on Plastic Rotational Capacity of Reinforced Concrete Beams

by Alberto Carpinteri, Mauro Corrado, Giuseppe Mancini, and Marco Paggi

A complete numerical algorithm that assumes a strain localization in concrete, both in tension and compression, is proposed for modeling cracking and crushing growths during the loading process of reinforced concrete beams in bending. With this algorithm based on nonlinear fracture mechanics models, it is possible to investigate the effects of the main mechanical and geometrical parameters on the rotational capacity with particular regard to the reinforcement percentage and the element size. A comparison with experimental results demonstrates the effectiveness of the proposed approach for a wide range of reinforcement percentages and beam depths. The obtained results show that the prescriptions concerning the admissible plastic rotations provided by the existing design formulas are not conservative in the case of large structural sizes. To overcome such a drawback, a new design diagram is proposed for practical purposes.

Keywords: code provisions; cohesive crack model; ductility; finite element method; nonlinear analysis; plastic rotation; reinforced concrete; size effect.

INTRODUCTION

The development of considerable ductility in the ultimate limit state is a key parameter for the design of reinforced concrete (RC) beams in bending.[1-6] The interest in ductility was formerly connected with the diffusion of plastic analysis in the design of RC structures.[2,7,8] In this context, in fact, the rotational capacity is required to allow the bending moment redistribution in statically indeterminate structures. The ductility contributes to satisfy many other requirements necessary to guarantee the structural safety, as, for example, robustness, warning of incipient collapse by the development of large deformation prior to collapse, and development of major distortions and energy dissipation during earthquakes.

Due to the complexity of the phenomenon, the first contribution to the study of the rotational capacity derives from the experimental programs coordinated by the Indeterminate Structures Commission of the Comité Européen du Béton[9] in the early 1960s. Several tests were carried out in different laboratories and countries. The results, published in 1967,[8] led to the proposal of a hyperbolic relationship between plastic rotation ϑ_{PL} and relative neutral axis depth x/d

$$\vartheta_{PL} = \frac{0.004}{x/d} \tag{1}$$

where x is the distance of the neutral axis from the compressed edge at the ultimate condition; and d is the effective depth of the beam cross section.

This expression was assumed by the first versions of the codes, as, for example, in Model Code 78, to solve the problem of plastic rotation evaluation for practical purposes.

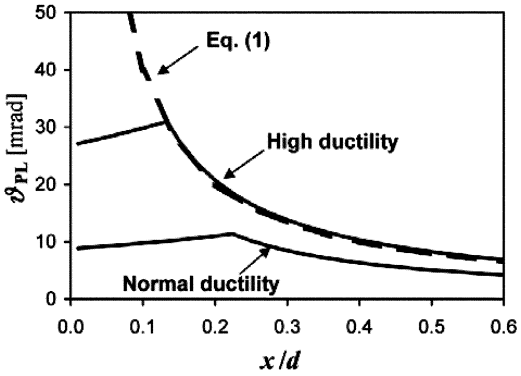

Fig. 1—Evolution of design formula for evaluation of plastic rotation.

A second fundamental contribution comes from the research carried out in the early 1980s at the University of Stuttgart by the group coordinated by R. Eligehausen.[4,10] In their studies, an analytical model was developed to describe the behavior of plastic hinges, considering that the final collapse can be achieved either by steel rupture or by concrete crushing. In Fig. 1, where the provisions of Eq. (1) are compared with the Stuttgart proposal, two aspects have to be highlighted: first, the increasing branch for low values of x/d due to steel rupture; and, second, the explicit consideration of two classes of reinforcement with different ductility properties.

Further improvement in the analysis of the behavior of RC members in bending was marked by the pioneering paper by Hillerborg in 1990,[5] who introduced the concept of strain localization in concrete in compression. According to his approach, when the ultimate compressive strength is achieved, a strain localization takes place within a characteristic length proportional to the depth of the compressed zone. This model allows the issue of size effects to be addressed, although the definition of the length over which the strain localization occurs is a free parameter and its value is not defined on the basis of theoretical arguments. Afterward, several models have been developed on the basis of the Stuttgart and the Hillerborg proposals, emphasizing some more specific aspects.[11-15]

To assess the rotational capacity of RC beams, Eurocode 2[16] provides a design diagram relating the admissible plastic rotation to the relative neutral axis position (refer to Fig. 2). The dotted lines refer to high-ductility steel, while the solid lines refer to normal-ductility steel. From the analysis of

ACI Structural Journal, V. 106, No. 6, November-December 2009.

MS No. S-2008-340 received October 17, 2008, and reviewed under Institute publication policies. Pertinent discussion including author's closure, if any, will be published in the September-October 2010 *ACI Structural Journal* if the discussion is received by May 1, 2010.

Alberto Carpinteri *is a Professor of structural mechanics at the Politecnico di Torino, Torino, Italy. His research interests include strength of materials, fracture mechanics, structural integrity, framentation and comminution, advanced composite materials, acoustic emission, and spatio-temporal scale effects in the mechanics and physics of solid materials.*

Mauro Corrado *is a Post-Doctoral Fellow of structural design at the Politecnico di Torino. His research interests include fracture mechanics of concrete and reinforced concrete structures and nonlinear behavior of reinforced concrete structures.*

ACI member **Giuseppe Mancini** *is a Professor of structural design at the Politecnico di Torino. His research interests include nonlinear behavior of reinforced concrete structures, structural safety assessment, reinforcement corrosion, bridge design, and design models.*

Marco Paggi *is an Assistant Professor of structural mechanics at the Politecnico di Torino. His research interests include fracture mechanics and contact mechanics, including stress singularities in elasticity, contact mechanics of rough surfaces, interface constitutive laws, finite element analysis in contact and fracture mechanics, fracture of functionally graded materials, damage and fracture phenomena in cutting tools, scaling laws in fatigue, and nonlinear behavior of concrete structures.*

these curves, it appears that the size-scale effects on the rotational capacity of RC beams are not considered, although the dependence of the structural dimension was recognized in several experimental tests.[1,6,17-19]

In the case of concrete specimens subjected to uniaxial compression, several experiments[20-23] reveal that the size-scale effects are due to two interconnected phenomena: the strain localization after the peak load and the consequent energy dissipation over a surface, the value of which (referred to as a unitary surface) can be considered as a material parameter. More precisely, such an energy generally depends on the lateral confinement and, hence, on the level of restraint imposed by the test equipment to the specimen lateral deformation. For this reason, the true material property can be experimentally evaluated only if friction-reducing measures are adopted[24-26] or if specimens with slenderness higher than 2.5 are tested.[23] Based on this evidence, Carpinteri et al.[27,28] have recently proposed to model the process of concrete crushing using an approach analogous to the cohesive crack model, which is routinely adopted for modeling the tensile behavior of concrete. The former approach is referred to as the "overlapping crack model,"[27,28] which assumes a stress-displacement law for the post-peak behavior. In tension, the localized displacement is represented by a crack opening, while in compression it would be represented by an interpenetration, as clearly shown in Fig. 3.

In this paper, a new numerical method able to describe the nonlinear behavior of RC members during both fracturing and crushing is proposed. First, the cohesive crack model for concrete in tension and the overlapping crack model for concrete in compression are introduced, as well as the stress-displacement relationship for steel in tension. Then, a numerical algorithm based on the finite element method is presented for the analysis of intermediate situations ranging from pure concrete members to over-reinforced beams. It is assumed that the fracturing and crushing processes are fully localized along the midspan cross section of the representative structural element in bending. This assumption, fully consistent with the physics of the crushing phenomenon, also implies that only one equivalent main tensile crack is considered. To validate the proposed model, a comparison between the numerical predictions and the experimental results for the beams tested by Bosco and Debernardi[18] is carried out. Finally, as a result of a parametric investigation on the influence of the structural dimension and of the steel percentage, a comparison with the prescription of the Eurocode 2[16] is reported

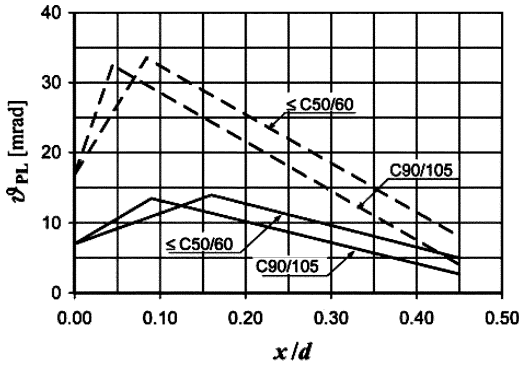

Fig. 2—Plastic rotation versus relative neutral axis position relationships provided by Eurocode 2.[16]

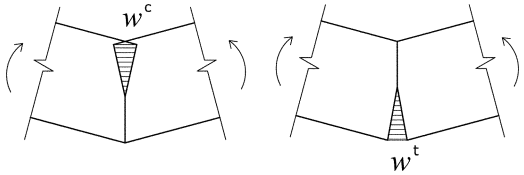

Fig. 3—(a) Compression crushing with overlapping; and (b) analogous tensile fracture with cohesive zone.

in terms of plastic rotation as a function of the relative neutral axis position. Future developments and perspectives of the proposed model conclude the paper.

RESEARCH SIGNIFICANCE

Most of the prescriptions provided by international codes about the rotational capacity of RC elements do not take into account the influence of the structural dimension. On the other hand, a significant size-scale effect on the plastic rotation of RC beams in bending has been noticed by several experimental tests.[1,6,17-19] The model proposed in this paper for the evaluation of the rotational capacity of RC members represents a step forward with respect to the existing models for the description of the mechanical behavior of RC beams in bending. Based on the assumption of strain localization, both in tension and in compression, insight into the problem of size-scale effects is given. This will show the limitations of the prescriptions of the existing design codes and provide methods to overcome them.

EXPERIMENTAL INVESTIGATION

The testing program considered herein was carried out in the Materials and Structures Laboratory of the Department of Structural Engineering and Geotechnics of the Politecnico di Torino by Bosco and Debernardi[18] on 11 simply supported RC beams. The dimensional classes with the corresponding reinforcement percentages in tension and compression and the stirrups amount analyzed are given in Table 1. The beam slenderness $L/h = 10$, the effective depth to total depth ratio $d/h = 0.9$, and the diameter of the tension bars, $\phi = 12$ mm (0.47 in.), were kept constant. The beams were loaded by one concentrated force applied at the midspan position, as shown in Fig. 4. The tests were performed under displacement-control by imposing a midspan deflection until complete beam failure. The instrumentation included two linear potentiometers (Devices 7 and 12 in Fig. 4) for measuring the deformations

Table 1—Characteristics of beams tested by Bosco and Debernardi[18]

Beam	*h*, mm (in.)	*b*, mm (in.)	*L*, mm (in.)	Tension reinforcement, %	Compression reinforcement, %	Stirrups
T1	200 (7.87)	100 (3.93)	2000 (78.74)	0.57	0.25	ϕ6/150
T2				1.13	0.50	
T3				1.71	0.50	
T4	400 (15.74)	200 (7.87)	4000 (157.48)	0.28	0.20	ϕ6/200
T5				0.57	0.20	
T6				1.13	0.20	
T7				1.71	0.30	
T8	600 (23.62)	300 (11.81)	6000 (236.22)	0.13	0.12	ϕ6/150
T9				0.25	0.12	
T10				0.57	0.12	
T11				1.13	0.12	

at the top and bottom sides of the beam. The length of each extensometer is equal to the beam depth. By means of such an instrumentation, the rotation of the midspan portion, characterized by a length-to-depth ratio equal to 1, can be directly evaluated as the difference between the longitudinal displacements at the soffit and at the extrados, divided by the beam depth.

Two types of steel with different mechanical properties were used for the reinforcing bars: high ductility-steel (B 500 H), and normal-ductility steel (B 500 N), according to the specification given in the Eurocode 2.[16] The mean concrete compressive and tensile strengths were equal to 30.9 and 2.97 MPa (4.48 and 0.43 ksi), respectively.

NUMERICAL INVESTIGATION

In this section, a new model based on fracture mechanics concepts is proposed for the evaluation of the rotational capacity of RC beams in bending. A portion of an RC beam subjected to a bending moment M is considered. This element, having a span-depth ratio equal to unity, is assumed to be representative of the central zone of the beam where a plastic hinge formation takes place. This is always the case where a severe gradient in the bending moment diagram exists, as, for example, in the midspan position of three-point bending tests or in the internal supports of continuous beams. Note, incidentally, that the analysis of this structural element is also consistent with the prescriptions reported in Eurocode 2.[16] It is assumed that the midspan cross section of this element is fully representative of its mechanical behavior. The stress distribution is linear-elastic until the tensile stress at the soffit reaches the concrete tensile strength. When this threshold is reached, a cohesive crack propagates from the beam soffit toward its extrados. Correspondingly, the applied moment increases. Outside the crack, the material is assumed to behave linear-elastically. According to the well-known cohesive crack model,[29,30] the stresses in the cohesive zone are assumed to be decreasing functions of the crack opening displacement until a critical value of crack opening is reached.

On the other hand, the damage phenomenon leading to concrete crushing begins when the maximum stress in compression reaches the concrete compressive strength. Afterward, the development of microcracking up to full fragmentation takes place with a subsequent reduction of the stresses in the compression zone. Damage is then described as a fictitious interpenetration of the two half-beams,

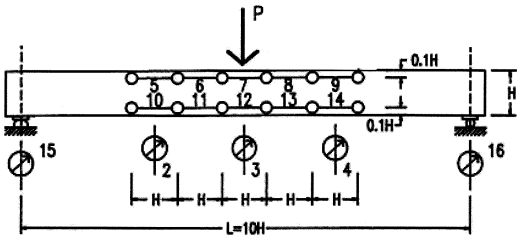

Fig. 4—Testing scheme and loading condition for beams tested by Bosco and Debernardi.[18]

representing the localization of the dissipated energy. The larger the interpenetration (also referred to as overlapping in the sequel) is, the lower the transferred forces along the damaged zone.

Cohesive crack model for description of concrete fracturing

A pioneering model for the analysis of nonlinear crack propagation in concrete was proposed by Hillerborg et al.[29,30] with the name of "fictitious crack model." Subsequently, an updated algorithm was implemented by Carpinteri,[31,32] referred to as "cohesive crack model," to study the ductile-to-brittle transition and the snap-back instability in plain concrete beams in bending. According to this model, the constitutive law used for the nondamaged zone is a σ-ε linear-elastic relationship up to the tensile strength σ_u. In the process zone, the damaged material is still able to transfer a tensile stress across the crack surfaces. The cohesive stresses are considered to be decreasing functions of the crack opening w^t, as follows

$$\sigma = \sigma_u \left(1 - \frac{w^t}{w^t_{cr}} \right) \tag{2}$$

where w^t is the crack opening; w^t_{cr} is the critical value of the crack opening corresponding to the condition $\sigma = 0$ ($w^t_{cr} \approx 0.1$ mm [0.004 in.]); and σ_u is the tensile strength of concrete. The area under the stress-versus-displacement curve represents the fracture energy G_F.

Overlapping crack model for description of concrete crushing

The most frequently adopted constitutive laws for concrete in compression describe the material behavior in terms of stress and strain (elastic-perfectly plastic, parabolic-perfectly plastic, and Sargin's parabola). Such approaches imply that the energy is dissipated within a volume, whereas experimental results reveal that the energy is substantially dissipated over a surface as a result of strain localization, regardless of the specimen geometry.[20-23] The actual failure mode and the energy dissipation of concrete specimens in uniaxial compression is extremely complex and dependent on the loading conditions and on the specimen size-scale and slenderness.[24-26] For instance, longitudinal or inclined cracks may appear, respectively, in the case of splitting or shear failure, as observed in slender and/or large specimens. In the opposite geometrical configurations, the development of a transversal dissipation band takes place due to crushing failure. All of these failure modes exhibit a strong longitudinal strain localization. Hillerborg[5] first proposed to model the crushing phenomenon as a strain localization over a length

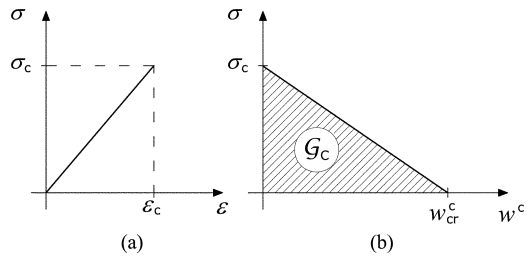

Fig. 5—Concrete constitutive law in compression: (a) σ–ε linear-elastic law; and (b) σ-w post-peak softening law.

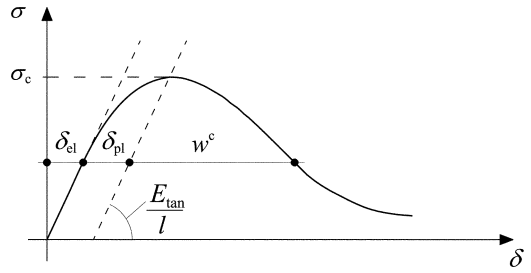

Fig. 6—Evaluation of localized interpenetration w^c *from total shortening of specimen, δ.*

proportional to the depth of the compressed zone. The evaluation of this characteristic length, however, is rather complicated because the depth of the compressed zone is not a constant, but varies during the loading process. This condition, however, does not allow formulating a material constitutive law fully describing the mechanical response of concrete in compression. The assumption of strain localization in compression was also experimentally confirmed by van Vliet and van Mier[22] and by Jansen and Shah[23] for concrete and by Hudson et al.,[33] until 1972, for rocks.

In the present formulation, we adopt the stress-displacement relationship proposed by Carpinteri et al.[27] and then considered by Corrado,[28] between the compression stress and the interpenetration, in close analogy with the cohesive model. The main hypotheses are:

1. The constitutive law used for the undamaged material is a linear-elastic stress-strain relationship (refer to Fig. 5(a)).

2. The crushing zone develops perpendicular to the principal compression stress, when it reaches the concrete compressive strength.

3. The damaged material in the process zone is assumed to be able to transfer compression stresses between the overlapping surfaces. They are assumed to be decreasing functions of the interpenetration, w^c (refer to Fig. 5(b))

$$\sigma = \sigma_c\left(1 - \frac{w^c}{w^c_{cr}}\right) \tag{3}$$

where w^c is interpenetration, w^c_{cr} is the critical value of the interpenetration corresponding to the condition of $\sigma_c = 0$, and σ_c is the compressive strength.

From an experimental point of view, the post-peak σ-w^c relationship is determined by subtracting the elastic elongation, caused by the reduction of the applied stress in the post-peak regime, δ_{el}, and the pre-peak plastic deformation, δ_{pl}, from the σ-δ diagram (refer to Fig. 6). The value of the displacement δ_{el} is given by the following expression

$$\delta_{el} = \frac{\sigma}{E_{tan}} l \tag{4}$$

where σ is the actual value of the compression stress, E_{tan} is the tangent elastic modulus, and l is the specimen length.

The crushing zone is then represented by a fictitious overlapping, which is mathematically analogous to the fictitious crack in tension, as shown in Fig. 3. The results by Jansen and Shah[24] show that, regardless of the failure mode of concrete specimen in uniaxial compression tests, the concept of overlapping crack can be profitably applied to predict the mechanical response even when inclined shear bands develop. In the present context, the main novelty of the proposed model is the generalization of this concept to the analysis of the behavior of RC beams in bending. In this field, most of the available models require a detailed description of the triangular-shaped wedge, which is expelled during crushing (for example, Fantilli et al.[15]). With respect to such approaches, our proposed model allows us to avoid the elaborate description of the kinematics of the failure mode.

It is worth noting that the crushing energy G_C, defined as the area below the post-peak softening curve of Fig. 5(b), is now a true material parameter, because it is not affected by the structural dimension. The following empirical formulation for calculating the crushing energy has recently been proposed by Suzuki et al.,[34] based on the results of compression tests carried out on plain and transversely reinforced concrete specimens

$$\frac{G_C}{\sigma_c} = \frac{G_{C,0}}{\sigma_c} + 10{,}000\frac{k_a^2 p_e}{\sigma_c^2} \tag{5}$$

where σ_c is the average concrete compressive strength, in N/mm^2, k_a is the parameter depending on the stirrups strength and on the volumetric percentage, and p_e is the effective lateral pressure.

Equation (5) allows one to evaluate the effect of the confinement exerted by the stirrups on the ductility of concrete in compression. On the other hand, the crushing energy of the unconfined concrete, $G_{C,0}$, can be calculated using the following expression, proposed again by Suzuki et al.[34]

$$G_{C,0} = 80 - 50k_b \tag{6}$$

where the parameter k_b depends on the concrete compressive strength.

A comparison between crushing energy and fracture energy for different compressive strengths is proposed in Table 2. The crushing energy is calculated according to Eq. (6) for concrete without stirrups, while the fracture energy is calculated according to the CEB-FIP Model Code 90[35] in case of a maximum aggregate dimension of 16 mm (0.63 in.). It is worth noting that G_C is between two and three orders of magnitude higher than G_F. Finally, the critical value for crushing interpenetration of normal-strength concrete is approximately equal to $w_{cr}{}^c \approx 1$ mm (0.04 in.) (see also the experimental results by Jansen and Shah[23]). This property, however, depends on the compressive strength and on the crushing energy. In particular, high-strength concrete, which exhibits a more brittle mechanical response than normal-strength concrete, has a critical value of interpenetration

Table 2—Comparison between crushing energy and fracture energy as function of concrete compressive strength

σ_c, N/mm^2 (ksi)	$G_{C,0}$, N/mm (lbf/in.)	G_F, N/mm (lbf/in.)
30 (4.35)	30 (171.3)	0.065 (0.37)
50 (7.25)	40 (228.4)	0.090 (0.51)
70 (10.15)	51 (291.21)	0.117 (0.67)
90 (13.05)	58 (331.18)	0.140 (0.80)

lower than 1 mm (0.04 in.). On the contrary, it is an increasing function of the crushing energy for a given compressive strength.

Steel-concrete interaction

The constitutive laws usually adopted in practice to model the steel contribution to the load-carrying capacity of RC beams are defined in stress-versus-strain diagrams, as, for example, the well-known elasto-plastic and elasto-hardening relationships. In the model proposed in this paper, it is not possible to adopt such laws because the kinematics of the midspan cross section of the RC member is described by means of displacements instead of strains. Consequently, a constitutive relationship between reinforcement reaction and crack opening displacement has to be introduced. In the past, this problem has been overcome by assuming a rigid-plastic behavior for steel.[36] This assumption involves that the crack opening is zero up to the steel yielding. Then, the reinforcement reaction is constant. In the proposed model, a stress versus crack opening relationship for steel reinforcement has been obtained by means of preliminary studies carried out on the interaction between the steel and the surrounding concrete. On the basis of the bond-slip relationship provided by Model Code 90,[35] and by imposing equilibrium and compatibility conditions, it is possible to correlate the reinforcement reaction to the relative slip at the crack edge, which corresponds to half the crack opening displacement. Typically, the obtained relationship is characterized by an ascending branch up to steel yielding, corresponding to a critical value of the crack opening, w_y, after which the steel reaction is nearly constant. In the present algorithm, this stress-displacement law has been introduced in input, together with the cohesive and overlapping constitutive laws.

Numerical algorithm

A discrete form of the elastic equations governing the mechanical response of the two half-beams is herein introduced in order to develop a suitable algorithm for the analysis of intermediate situations where both fracturing and crushing phenomena take place. According to the finite element method, the midspan cross section of the RC member having the length-to-depth ratio equal to unity is subdivided into finite elements with n nodes (Fig. 7). In this scheme, cohesive or overlapping stresses are replaced by equivalent nodal forces by integrating the corresponding tractions or pressures over each finite element size. Such nodal forces depend on the nodal opening or closing displacements according to the cohesive or overlapping softening laws previously introduced.

With reference to Fig. 7, the horizontal forces F acting along the midspan cross section are given by

$$\{F\} = [K_w]\{w\} + \{K_M\}M \tag{7}$$

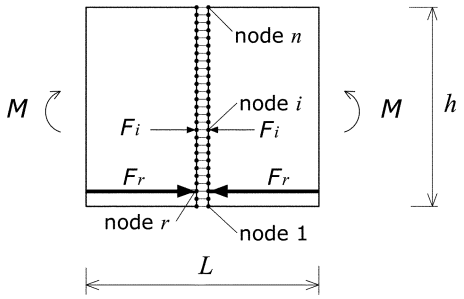

Fig. 7—Finite element nodes along middle cross section.

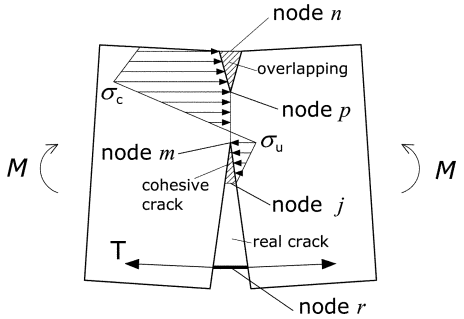

Fig. 8—Force distribution with cohesive crack in tension and fictitious interpenetration in compression.

where $\{F\}$ is the vector of nodal forces; $[K_w]$ is the matrix of the coefficients of influence for the nodal displacements; $\{w\}$ is the vector of nodal displacements; $\{K_M\}$ is the vector containing the coefficients of influence for the applied moment; and M is the applied moment.

The coefficients of influence, $[K_w]$, present the physical dimension of a stiffness and are computed a priori with a finite element analysis by applying a unitary displacement to each of the nodes shown in Fig. 7 (refer to the Appendix). The reinforcement contribution is also included in the nodal force corresponding to the r-th node.

In the generic situation shown in Fig. 8, the following equations can be considered

$$F_i = 0 \quad \text{for } i = 1, 2, ..., (j-1);\ i \neq r \tag{8a}$$

$$F_i = F_u\left(1 - \frac{w_i^t}{w_{cr}^t}\right) \quad \text{for } i = j, ..., (m-1);\ i \neq r \tag{8b}$$

$$w_i = 0 \quad \text{for } i = m, ..., p \tag{8c}$$

$$F_i = F_c\left(1 - \frac{w_i^c}{w_{cr}^c}\right) \quad \text{for } i = (p+1), ..., n \tag{8d}$$

$$F_r = f(w_r) \quad \text{for } i = r \tag{8e}$$

Equation (8e) represents the relationship between the closing force exerted by the reinforcing steel and the crack opening at the reinforcement level. Such a law is determined on the basis of the bond-slip behavior of concrete and steel.

Equations (7) and (8) constitute a linear algebraic system of $(2n)$ equations and $(2n + 1)$ unknowns, namely, $\{F\}$, $\{w\}$,

Table 3—Flowchart of proposed numerical algorithm

```
LOOP crack and crushing propagation
        INIZIALIZE M=Mold+1
        SOLVE the system of Eqs. (5) and (6)
        IF (Fc−Fp)/Fc < (Fu−Fm)/Fu
                THEN: crack propagation prevails (crisis=1)
                ELSE: crushing propagation prevails (crisis=2)
        END IF
        LOOP over iterations: i = 1, …, convergence (Fm=Fu IF crisis=1 or Fp=Fc IF crisis=2)
        UPDATE the value of M
                SOLVE the system of Eqs. (5) and (6)
        END
        PROPAGATE the fictitious crack tip (IF crisis=1) or the fictitious overlapping tip (IF crisis=2) of one
                finite element node
END
```

and M. The necessary additional equation derives by the stress criterion adopted to govern the propagation processes. It is important to note that cracking and crushing phenomena are physically independent of each other. As a consequence, the condition for crack propagation (corresponding to the achievement of the tensile strength at the fictitious crack tip, m) does not imply that the compressive strength is reached at the corresponding overlapping crack tip, p, and vice versa. Hence, at each step of the algorithm, the values of the tensile and overlapping fictitious crack tip nodal forces are compared with the corresponding critical quantities for propagation, as schematically shown in the flowchart reported in Table 3. This comparison is performed to establish which phenomenon would prevail. The driving parameter of the process is the position of the fictitious tip that in the considered step has reached the limit resistance. Only this tip is moved of one node when passing to the next step.

The two fictitious tips advance until they converge to the same node. Thus, to describe the descending branch of the moment-rotation diagram, the two tips can move together toward the beam intrados. As a consequence, the crack in tension closes and the overlapping zone is allowed to extend toward the intrados. In these conditions, a further propagation of the tensile crack toward the extrados has to be excluded. In fact, this would correspond to a reduction of the compressed zone, making it impossible to satisfy the longitudinal equilibrium equation of the forces acting across the beam cross section. This situation is commonly observed in over-reinforced beams, where steel yielding does not take place.

Finally, at each step of the algorithm, it is possible to calculate the beam rotation ϑ as follows

$$\vartheta = \{D_w\}^T\{w\} + D_M M \tag{9}$$

where $\{D_w\}$ is the vector of the coefficients of influence for the nodal displacements, with physical dimension of $[L]^{-1}$; and DM is the coefficient of influence for the applied moment, with physical dimension of $[F]^{-1}[L]^{-1}$.

COMPARISON OF PREDICTIONS AND EXPERIMENTAL RESULTS

In this section, a comparison between the numerical predictions using the cohesive/overlapping crack model and the experimental results of the tests carried out by Bosco and Debernardi[18] is proposed. To obtain a consistent comparison, the numerical simulations have been carried out by modeling the beam portion positioned at the midspan of the beam shown in Fig. 4. Such an element is characterized by a span-depth ratio equal to 1. The rotations of such a portion, where the largest amount of ductility is developed, were experimentally determined as functions of the applied bending moment. In the numerical scheme, the midspan

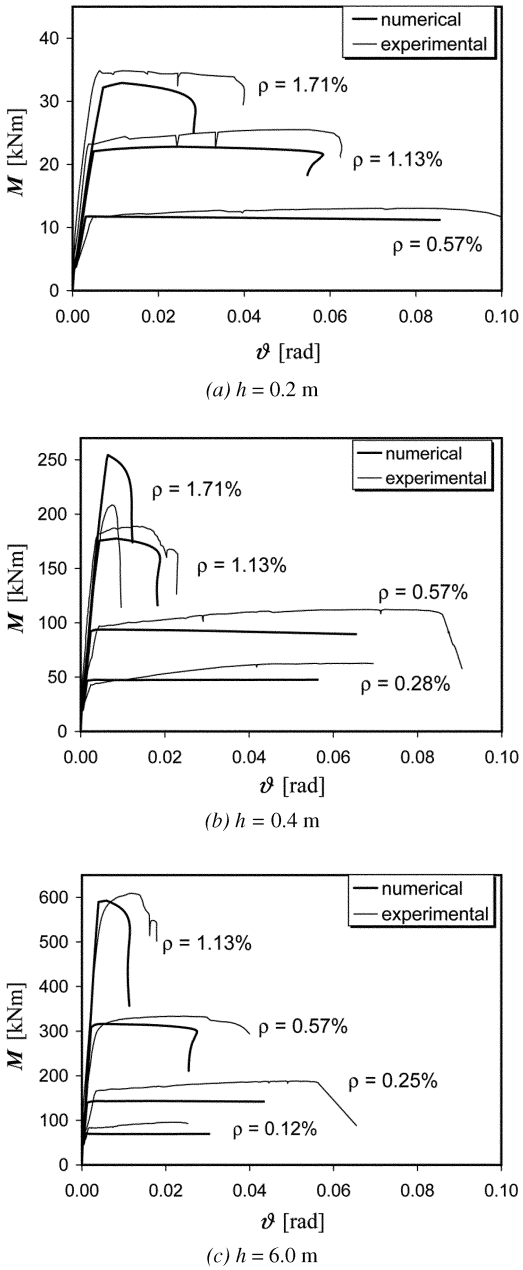

Fig. 9—Comparison between numerical and experimental results[18] for different beam depths.

cross section of this element is discretized into 160 elements and the coefficients of influence entering Eq. (6) are preliminarily determined using the finite element method. The mechanical and geometrical parameters are set equal to the experimental values. Numerical and experimental moment-rotation curves are then compared in Fig. 9(a) to (c) for different beam depths and different steel percentages. It is worth noting that, from the numerical point of view, the beam rotation is computed exactly as in the experiments, that is, as the difference between the longitudinal displacements at the soffit and at the extrados of the opposite edges of the beam portion, divided by the beam depth. The diagrams in Fig. 9(a) to (c) put into evidence that the maximum rotation is a decreasing function of the tensile reinforcement ratio and of the beam depth. In the case of low steel percentages, the mechanical behavior is characterized by the reinforcement yielding, and the mechanical response is almost plastic. By

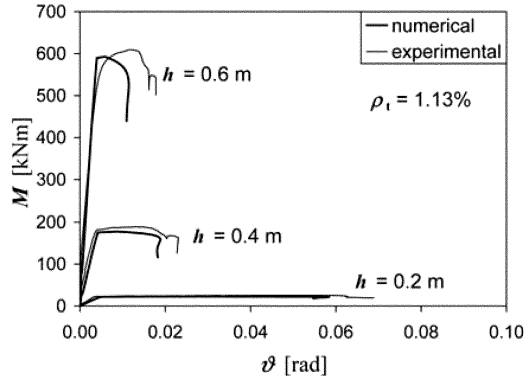

Fig. 10—Comparison between numerical and experimental results[18] for ρ_t = 1.13%.

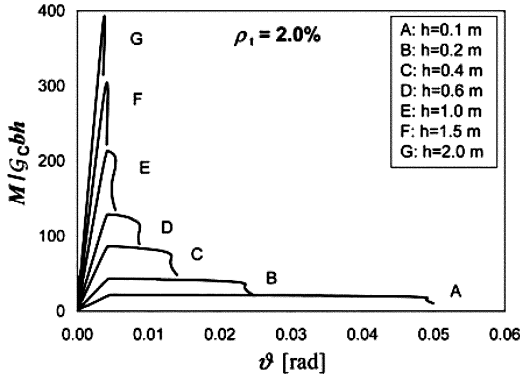

Fig. 11—Nondimensional bending moment versus total rotation diagrams for ρ_t = 2% by varying the beam depth.

increasing the amount of reinforcement, the contribution of concrete crushing becomes more and more evident with the appearance of a softening branch at the end of the plastic plateau. This is an important feature of the proposed model, which also permits to follow unstable softening branches with positive slopes (snap-back) by controlling the loading process through the length of the tensile crack and the extension of the fictitious crushing zone, rather than by the external load. In Fig. 10, the size-scale effect is evidenced by keeping constant the steel percentage equal to 1.13% and varying the beam depth from 0.2 to 0.6 m (7.87 to 23.62 in.). Good agreement was obtained between numerical and experimental results for all the tested beams.

NUMERICAL RESULTS AND DISCUSSION

After a model validation by means of the comparison proposed in the previous section, a parametric analysis is carried out to investigate the influence of two fundamental parameters affecting the global mechanical behavior of RC beams in bending, namely, the beam size and the steel percentage. The length-to-depth ratio and the thickness b of the considered beam portion are kept constant in the following examples and are equal to 1 and 0.2 m (39.35 and 7.87 in.), respectively. The following mechanical parameters are assumed for concrete: σ_c = 40 MPa (5.80 ksi); G_C = 30 N/mm (171.3 lbf/in.); σ_u = 4 MPa (0.58 ksi); and G_F = 0.08 N/mm (0.46 lbf/in.). The tensile yield strength of steel, f_y, is set equal to 400 MPa (58.01 ksi). In the present study, the critical opening displacement at the reinforcement level, w_y, has been set equal to 0.3 mm (0.0118 in.) in all the numerical simulations. This reasonable assumption has allowed us to obtain a good agreement with the experimental rotations corresponding to the yielding point (refer to Fig. 9 and 10). In the parametric study, the reinforcement ratio ρ_t has been varied from 0 to 3%, whereas the beam depth h has been varied from 0.1 to 2.0 m (3.97 to 79.36 in.). It is worth noting that a subdivision of the midspan cross section in 160 finite elements, which corresponds to a nodal spacing ranging from 0.625×10^{-3} m (0.0246 in.) for the beam depth equal to 0.1 m (3.97 in.), to 12.5×10^{-3} m (0.492 in.) for the beam depth equal to 2.0 m (79.36 in.) was adequate to avoid any convergence problem.

The typical trend obtained by varying the beam depth is that reported in Fig. 11 in the case of tensile reinforcement percentage equal to 2.0%. A plateau is observed in the nondimensional bending moment versus rotation diagram when steel yielding occurs. These curves put into evidence that the beam rotation at failure is progressively diminished by increasing the beam depth, with the appearance of steeper and steeper snap-back branches. A feature of the proposed model is that it is not necessary to introduce any hypotheses on the deformation field, unlike, for example, the Bernoulli hypothesis. On the contrary, the true nodal displacements at the midspan cross section are obtained through the step-by-step numerical solution. The nodal displacements' profiles in the case of beam depth equal to 0.4 m (15.75 in.) and amount of reinforcement equal to 2% are shown in Fig. 12 for different values of the applied bending moment. For low values of the applied moment, up to approximately 60% of the yielding bending moment, the mechanical behavior is characterized by a progressive advancing and opening of the tensile crack. The concrete crushing starts to develop just before the yielding moment and it becomes more and more evident by approaching the ultimate moment.

With reference to the moment-rotation diagrams, the plastic component of the total rotation can be obtained as the difference between the ultimate rotation and the rotation corresponding to the reinforcement yielding, as shown in Fig. 13. According to the definition proposed by Hillerborg[5] and Pecce,[37] the ultimate rotation is the rotation beyond which the moment starts descending sharply. This occurrence can be easily identified in our numerically predicted curves.

The results of the parametric analysis can be summarized in a plastic rotation versus relative neutral axis position (x/d) diagram. This is also consistent with the practical prescriptions of the codes of practice. The numerical results referred to different beam depths are compared in Fig. 14 with the curve provided by Eurocode 2[16] for high-ductility steel and concrete compressive strength less than or equal to 50 MPa (7.25 ksi). Beams with a depth equal to 0.2 m (7.87 in.) have a rotational capacity greater than that suggested by the code, whereas by increasing the beam depth up to 0.6 or 0.8 m (23.62 or 31.49 in.), the rotations provided by the code appear to be nonconservative. It is worth noting that the numerical results are substantially in good agreement with the curve provided by the code, because the latter was calibrated on a large series of tests carried out on beams with depth of approximately 0.3 m (11.81 in.).[38]

CONCLUSIONS

In the present paper, a numerical algorithm has been proposed for the analysis of the behavior of RC elements in bending. To this aim, the cohesive and the overlapping crack models have been merged to take into account all the principal nonlinear contributions influencing the moment-rotation

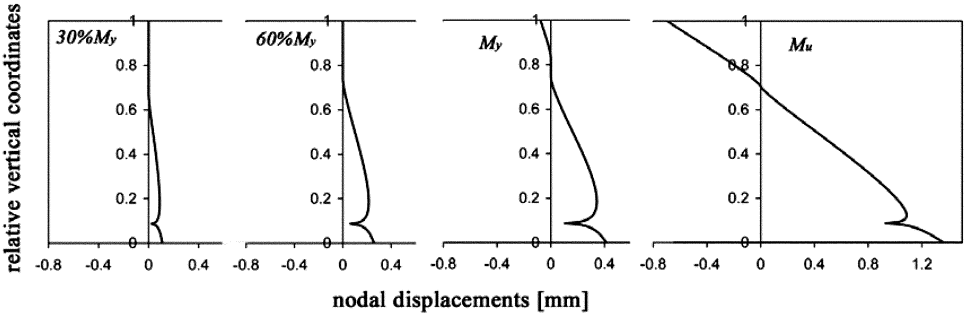

Fig. 12—Nodal displacement profiles at different applied moment for beam depth equal to 0.4 m and ρ_t = 2%. (Note: 1 mm = 0.0394 in.)

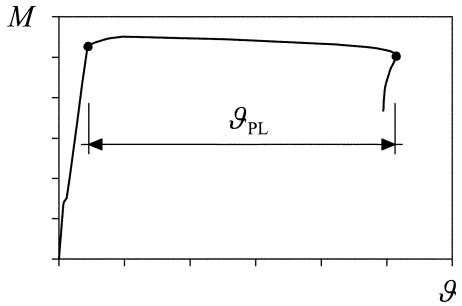

Fig. 13—Definition of plastic rotation.

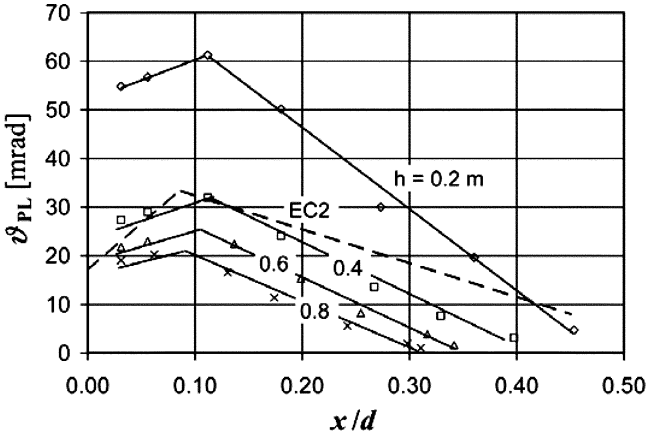

Fig. 14—Numerical plastic rotation for different beam depths (solid lines) compared with Eurocode 2 provisions (dotted line).

response. As a result, the proposed algorithm is very general and can be applied to all the intermediate situations ranging from plain to over-reinforced concrete beams. The focus of the present study, however, is the analysis of the rotational capacity. Hence, the fracture properties of concrete are almost negligible in this context because they mainly influence the ascending branch of the moment-rotation diagram and not the extension of the plastic plateau. On the contrary, it is worth noting that the size-scale effects on the rotational capacity are mainly caused by the nonlinearity of concrete in compression. The following main conclusions can be drawn from the comparison between numerical predictions and the experimental results:

1. The introduced constitutive law for concrete in compression through the overlapping crack model permits to describe the nonlinear behavior of concrete considering the effect of the structural dimension and to describe the descending branch of the moment-rotation diagram, as shown in Fig. 11. For large structural sizes and/or high reinforcement percentages, this softening branch can have a positive slope, leading to a snap-back instability.

2. Referring to Fig. 9 and 10, it is possible to state that the proposed algorithm catches the experimental results[18] by varying both the structural dimension and the steel percentage.

3. Independently of the reinforcement ratio, the behavior becomes more and more brittle by increasing the beam depth, with a progressive reduction of the ultimate rotation.

4. The parameters that mainly influence the rotational capacity of RC beams are: the concrete compressive strength, the crushing energy, the tensile and compressive reinforcement ratios (Fig. 9), as well as the beam size (Fig. 10 and 11). Marginal effects are due to the concrete tensile properties and the critical opening displacement at the reinforcement level.

According to Eurocode 2,[16] the plastic rotation of RC beams is considered to be a function of the neutral axis position only. On the contrary, the numerical results summarized in Fig. 14 show that this assumption leads to unconservative predictions for deep beams. To improve the code provisions, the effect of the structural dimension should be explicitly taken into account by considering different design curves, as, for instance, those proposed in Fig. 14. For a given value of *x/d* obtained from the application of the ultimate state analysis, the designer can enter Fig. 14 and determine different admissible plastic rotations as functions of the beam depth. These rotations have to be higher than those computed according to a step-by-step plastic structural analysis at ultimate load.

ACKNOWLEDGMENTS

The authors would like to acknowledge the financial support of the European Union to the Leonardo da Vinci Project "Innovative Learning and Training on Fracture (ILTOF)."

REFERENCES

1. Corley, G. W., "Rotational Capacity of Reinforced Concrete Beams," *Journal of the Structural Division*, ASCE, V. 92, 1966, pp. 121-146.

2. Macchi, G., "Limit-States Design of Statically Indeterminate Structures Composed of Linear Members," *Costruzioni in Cemento Armato*, Studi e Rendiconti, V. 6, 1969, pp. 151-191.

3. Siviero, E., "Rotation Capacity of Monodimensional Members in Structural Concrete," *CEB Bulletin d'Information*, No. 105, 1974, pp. 206-222.

4. Eligehausen, R., and Langer, P., "Rotation Capacity of Plastic Hinges and Allowable Moment Redistribution," *CEB Bulletin d'Information*, No. 175, 1987, pp. I7.9-I7.27.

5. Hillerborg, A., "Fracture Mechanics Concepts Applied to Moment Capacity and Rotational Capacity of Reinforced Concrete Beams," *Engineering Fracture Mechanics*, V. 35, 1990, pp. 233-240.

6. Bigaj, A. J., and Walraven, J. C., "Size Effect on Rotational Capacity of Plastic Hinges in Reinforced Concrete Beams," *CEB Bulletin d'Information* No. 218, 1993, pp. 7-23.

7. Macchi, G., "Elastic Distribution of Moments on Continuous Beams," *International Symposium on the Flexural Mechanics of Reinforced Concrete*, ASCE, Miami, FL, 1964, pp. 237-256.

8. Baker, A. L. L., and Amakarone, A. M. N., "Inelastic Hyperstatic Frame Analysis," *Proceedings of Conference on Flexural Mechanics of Reinforced Concrete*, SP-12, American Concrete Institute, Farmington Hills, MI, 1967, pp. 85-142.

9. Comité Euro-International du Béton, "Rapport de la Commission CEB 'Hyperstatiques'," *CEB Bulletin d'Information* No. 30, Lausanne, Switzerland, 1961.

10. Langer, P., "Verdrehfähigkeit Plastizierter Tragwerksbereiche im Stahlbetonbau," PhD thesis, University of Stuttgart, Institut für Werkstoffe im Bauwesen, DAfStb, Berlin, 1987, 199 pp.

11. Cosenza, E.; Greco, C.; and Manfredi, G., "La Valutazione Teorica di Spostamenti e Rotazioni in Fase Anelastica negli Elementi Monodimensionali in Cemento Armato," Atti dell'Accademia Nazionale dei Lincei, Serie IX, V. II, Fascicolo 3, 1991, pp. 249-258. (in Italian)

12. Tue, N.; Qian, L.; and Pommerening, D., "Abschlußbericht zum Forschungs vorhaben Duktilitätsanforderungen en vorgespannte Tragwerke im Hoch-, Grund- und Brückenbau," Technische Hochschule Darmstadt, Az. IV 1-5-683/92, 1996.

13. Bigaj, A. J., "Structural Dependence of Rotation Capacity of Plastic Hinges in RC Beams and Slabs," PhD thesis, Delft University, the Netherlands, 1998, 227 pp.

14. Bigaj, A. J., and Walraven, J., "Size Effects on Plastic Hinges of Reinforced Concrete Members," *Heron*, V. 47, 2002, pp. 53-75.

15. Fantilli, A. P.; Iori, I.; and Vallini, P., "Size Effect of Compressed Concrete in Four-Point Bending RC Beams," *Engineering Fracture Mechanics*, V. 74, 2007, pp. 97-108.

16. EN 1992-1-1, "Eurocode 2: Design of Concrete Structures—Part 1-1: General Rules and Rules for Buildings," 2003, Paragraph 5.6.

17. Mattock, A. H., "Rotational Capacity of Hinging Regions in Reinforced Concrete Beams," *Proceedings of Conference on Flexural Mechanics of Reinforced Concrete*, SP-12, American Concrete Institute/ American Society of Civil Engineers, 1967, pp. 143-181.

18. Bosco, C., and Debernardi, P. G., "Experimental Investigation on the Ultimate Rotational Capacity of R.C. Beams," *Report* No. 36, Atti del Dipartimento, Politecnico di Torino, Ingegneria Strutturale, 1992, 119 pp.

19. Markeset, G., "Failure of Concrete under Compressive Strain Gradients," PhD thesis, The Norwegian Institute of Technology, Trondheim, Norway, 1993, 168 pp.

20. van Mier, J. G. M., "Strain Softening of Concrete under Multiaxial Compression," PhD thesis, Eindhoven University of Technology, the Netherlands, Nov. 1984, 349 pp.

21. Dahl, H., and Brincker, R., "Fracture Energy of High-Strength Concrete in Compression," *Fracture of Concrete and Rock—Recent Developments*, S. P. Shah, S. E. Swartz, and B. Barr, eds., Elsevier Applied Science, England, 1989, pp. 523-536.

22. van Vliet, M., and van Mier, J., "Experimental Investigation of Concrete Fracture under Uniaxial Compression," *Mechanics of Cohesive-Frictional Materials*, V. 1, 1996, pp. 115-127.

23. Jansen, D. C., and Shah, S. P., "Effect of Length on Compressive Strain Softening of Concrete," *Journal of Engineering Mechanics*, V. 123, 1997, pp. 25-35.

24. RILEM TC 148-SSC, "Strain-Softening of Concrete in Uniaxial Compression," *Materials and Structures*, V. 30, 1997, pp. 195-209.

25. Carpinteri, A.; Ciola, F.; Pugno, N.; Ferrara, G.; and Gobbi, M. E., "Size-Scale and Slenderness Influence on the Compressive Strain-Softening Behaviour of Concrete," *Fatigue and Fracture of Engineering Materials and Structures*, V. 24, 2001, pp. 441-450.

26. Ferro, G., and Carpinteri, A., "Effect of Specimen Size on the Dissipated Energy Density in Compression," *Journal of Applied Mechanics*, V. 75, 2008, pp. 041003/1 to 041003/8.

27. Carpinteri, A.; Corrado, M.; Paggi, M.; and Mancini, G., "Cohesive versus Overlapping Crack Model for a Size Effect Analysis of RC Elements in Bending," *Fracture Mechanics of Concrete Structures*, A. Carpinteri, P. Gambarova, G. Ferro, G. Plizzari, eds., Taylor & Francis, London, UK, 2007, V. 2, pp. 655-663.

28. Corrado, M., "Effetti di scala sulla capacità di rotazione plastica di travi in calcestruzzo armato," PhD thesis, Politecnico di Torino, 2007, 164 pp. (in Italian)

29. Hillerborg, A.; Modeer, M.; and Petersson, P. E., "Analysis of Crack Formation and Crack Growth in Concrete by Means of Fracture Mechanics and Finite Elements," *Cement and Concrete Research*, V. 6, 1976, pp. 773-782.

30. Petersson P., "Crack Growth and Development of Fracture Zones in Plain Concrete and Similar Materials," *Report* TVBM-1006, Division of Building Materials, Lund Institute of Technology, 1981, 174 pp.

31. Carpinteri, A., "Interpretation of the Griffith Instability as a Bifurcation of the Global Equilibrium," *Application of Fracture Mechanics to Cementitious Composites*, S.P. Shah, ed., Martinus Nijhoff Publishers, Dordrecht, 1985, pp. 287-316.

32. Carpinteri, A., "Size Effects on Strength, Toughness, and Ductility," *Journal of Engineering Mechanics*, ASCE, V. 115, 1989, pp. 1375-1392.

33. Hudson, J. A.; Brown, E. T.; and Fairhurst, C. "Shape of the Complete Stress-Strain Curve for Rock," *Proceedings of the 13th Symposium on Rock Mechanics*, E. J. Cording, ed., American Society of Civil Engineers, New York, 1972, pp. 773-795.

34. Suzuki, M.; Akiyama, M.; Matsuzaki, H.; and Dang, T. H., "Concentric Loading Test of RC Columns with Normal- and High-Strength Materials and Averaged Stress-Strain Model for Confined Concrete Considering Compressive Fracture Energy," *Proceedings of the 2nd fib Congress*, Naples, Italy, June 5-8, 2006. (CD-ROM)

35. Comité Euro-International du Béton, "CEB-FIP Model Code 1990," Thomas Telford Ltd, Lausanne, *Bulletin* No. 213/214, 1993.

36. Bosco, C., and Carpinteri, A., "Softening and Snap-through Behaviour of Reinforced Elements," *Journal of Engineering Mechanics*, ASCE, V. 118, 1991, pp. 1564-1577.

37. Pecce, M., "Experimental Evaluation of Rotation Capacity of HPC Beams," *CEB Bulletin d'Information* No. 242, Comité Euro-International du Béton, Lausanne, 1997, pp. 197-210.

38. Eligehausen, R.; Fabritius, E.; Li, L.; and Zhao, R., "An Analysis of Rotation Capacity Tests," *CEB Bulletin d'Information* No. 218, Comité Euro-International du Béton, Lausanne, Switzerland, 1993, pp. 251-273.

APPENDIX

Equations (7) and (9) allow the fracturing and crushing processes of the midspan cross section to be analyzed by taking into account the elastic behavior of the reinforced concrete member. To this aim, all the elastic coefficients are computed a priori using a finite element analysis. In the present work, the finite element code FEAP, developed by R. Taylor at the University of California, Berkeley, CA, has been used. Due to the symmetry of the problem, a homogeneous concrete rectangular region, corresponding to half the tested specimen shown in Fig. 8, is discretized by means of quadrilateral plane stress elements with uniform nodal spacing. Horizontal constraints are then applied to the nodes along the vertical symmetry line (refer to Fig. A(a)). The coefficients $K_w^{i,j}$ entering Eq. (7), which relate the nodal force F_j to the nodal displacement w_i, have the physical dimensions of a stiffness and are computed by imposing a unitary horizontal displacement to each of the constrained nodes (Fig. A(b)). On the other hand, by applying a unitary external bending moment, it is possible to compute the coefficients K_M^i (Fig. A(c)). At the same time, each coefficient of influence for the nodal displacement on the global rotation, D_w^i, is given by the rotation of the free edge corresponding to a

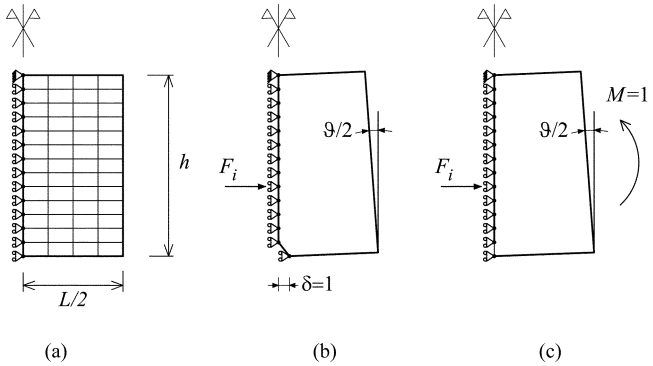

Fig. A—Scheme of finite element mesh (a) used for calculation of elastic coefficients (b) and (c). (One hundred sixty vertical subdivisions were used in numerical simulation.)

unitary displacement of the i-th constrained node. Finally, D_M is the rotation of the free edge corresponding to a unitary external bending moment.

As it relates to the analysis of beams characterized by different sizes, it has to observed that the coefficients entering Eq. (7) and (9) are connected by a simple relation of proportionality to the structural dimension. This means that it is not necessary to repeat the finite element analysis for any different considered beam size. More precisely, if all the three specimen sizes (depth h, span L, and thickness b) are multiplied by a factor k, then the coefficients are transformed as follows

$$K_w^{i,j}(kh) = kK_w^{i,j}(h) \tag{A1a}$$

$$K_M^i(kh) = \frac{1}{k}K_M^i(h) \tag{A1b}$$

$$D_w^i(kh) = \frac{1}{k}D_w^i(h) \tag{A1c}$$

$$D_M(kh) = \frac{1}{k^3}D_M(h) \tag{A1d}$$

On the other hand, if only depth and span are multiplied by the factor k, with the thickness being kept constant, then Eq. (A1a) and (A1d) are modified as follows

$$K_w^{i,j}(kh) = K_w^{i,j}(h) \tag{A2a}$$

$$D_M(kh) = \frac{1}{k^2}D_M(h) \tag{A2b}$$

while Eq. (A1b) and (A1c) are unchanged.